Supplementary Material:

All-liquid-crystal and full visible band tunable polarimetry

Guang-Yao Wang, [a] Han Cao, [a] Zheng-Hao Guo, [a]
Chun-Ting Xu, [a,*] Quan-Ming Chen, [a] and Wei Hu [a,*]

[a] National Laboratory of Solid State Microstructures, Key Laboratory of Intelligent Optical Sensing and Manipulation, College of Engineering and Applied Sciences, Nanjing University, Nanjing 210023, China

a) **Authors to whom correspondence should be addressed:** xuchunting@nju.edu.cn, and huwei@nju.edu.cn

Supplementary Note 1: Theoretical derivation of the proposed polarimeter.

Supplementary Note 2: The proposed polarimetry for polarization detection.

Supplementary Note 3: The *q*-plate array for polarization imaging.

Supplementary Note 1: Theoretical derivation of the proposed polarimeter.

The Jones matrix of the electrically tunable liquid crystal (LC), which is equivalent to a variable wave plate (VWP), can be indicated as

$$T = \cos(\frac{\Gamma_{\mathrm{VWP}}}{2})\mathrm{I} - i\sin(\frac{\Gamma_{\mathrm{VWP}}}{2})\begin{bmatrix}\cos(2m) & \sin(2m)\\ \sin(2m) & \text{-}\cos(2m)\end{bmatrix}, \tag{S1}$$

where I is the identity matrix, Γ_{VWP} is phase retardation of VWP and m is the azimuthal orientations of LC. Working at half-wave condition, the Jones matrix of the q-plate is

$$T_{q\text{-plate}} = -i\begin{bmatrix}\cos(2\alpha) & \sin(2\alpha)\\ \sin(2\alpha) & \text{-}\cos(2\alpha)\end{bmatrix}, \tag{S2}$$

where α is the azimuthal orientations of q-plate. Deviating from half-wave condition, the Jones matrix of the LCPG is

$$T_{\mathrm{LCPG}} = \cos(\frac{\Gamma}{2})\mathrm{I} - i\sin(\frac{\Gamma}{2})\begin{bmatrix}\cos(2\beta) & \sin(2\beta)\\ \sin(2\beta) & \text{-}\cos(2\beta)\end{bmatrix}, \tag{S3}$$

where Γ is the phase retardation of the LCPG.[16] Since polarized light can be divided into LCP ($|L\rangle$) and RCP ($|R\rangle$) components. The polarization state of light is expressed as

$$E = a_{\mathrm{L}}e^{i\varphi_{\mathrm{L}}}|L\rangle + a_{\mathrm{R}}e^{i\varphi_{\mathrm{R}}}|R\rangle = a_{\mathrm{R}}e^{i\varphi_{\mathrm{R}}}(re^{i\Delta\varphi}|L\rangle + |R\rangle), \tag{S4}$$

where a_{L} and a_{R} represent the amplitudes of LCP and RCP, $a_{\mathrm{L}}^2 + a_{\mathrm{R}}^2 = 1$, $r = a_{\mathrm{L}} / a_{\mathrm{R}}$, $r \in [0, +\infty)$ is the amplitude contrast; φ_{L} and φ_{R} represent the phases of orthogonal spins, $\Delta\varphi = \varphi_{\mathrm{L}} - \varphi_{\mathrm{R}}$, $\Delta\varphi \in [0, 2\pi]$ depicts the phase difference. After light passing through q-plate and LCPG successively, the electric field is indicated as

$$\begin{aligned} E'' &= T_{\mathrm{LCPG}} \cdot T_{q\text{-plate}} \cdot E \\ &= -i\cos(\frac{\Gamma}{2})(a_{\mathrm{L}}\mathrm{e}^{i\varphi_{\mathrm{L}}}\mathrm{e}^{i2\alpha}|R\rangle + a_{\mathrm{R}}\mathrm{e}^{i\varphi_{\mathrm{R}}}\mathrm{e}^{-i2\alpha}|L\rangle) - \sin(\frac{\Gamma}{2})a_{\mathrm{L}}\mathrm{e}^{i\varphi_{\mathrm{L}}}\mathrm{e}^{2i(\alpha-\beta)}|L\rangle - \sin(\frac{\Gamma}{2})a_{\mathrm{R}}\mathrm{e}^{i\varphi_{\mathrm{R}}}\mathrm{e}^{-2i(\alpha-\beta)}|R\rangle \end{aligned}. \tag{S5}$$

With a y-polarizer, the electric field of y-polarization is indicated as

$$\begin{aligned} \begin{bmatrix}0\\ E''_{y-po}\end{bmatrix} &= J_y \cdot E'' \\ &= \begin{bmatrix} 0 \\ \frac{\sqrt{2}}{2}\cos\frac{\Gamma}{2}(a_{\mathrm{L}}\mathrm{e}^{i\varphi_{\mathrm{L}}}\mathrm{e}^{i2\alpha} - a_{\mathrm{R}}\mathrm{e}^{i\varphi_{\mathrm{R}}}\mathrm{e}^{-i2\alpha}) + i\frac{\sqrt{2}}{2}\sin\frac{\Gamma}{2}a_{\mathrm{L}}\mathrm{e}^{i\varphi_{\mathrm{L}}}\mathrm{e}^{2i(\alpha-\beta)} - i\frac{\sqrt{2}}{2}\sin\frac{\Gamma}{2}a_{\mathrm{R}}\mathrm{e}^{i\varphi_{\mathrm{R}}}\mathrm{e}^{-2i(\alpha-\beta)} \end{bmatrix} \end{aligned}, \tag{S6}$$

where J_y is the Jones matrix of y-polarizer. The three items on the right side of Eq. (S6) exhibit 0^{th}, $+1^{\mathrm{st}}$ and -1^{st} orders, subsequently. After propagating a certain distance, the three orders are spatially

separated. The light field along the z-axis can be estimated by the approximation formula of Fresnel diffraction

$$E_y''(x,y,z)=\frac{ik_0}{2\pi z}\mathrm{e}^{ik_0 z}\iint E_{y-\mathrm{po}}''\cdot\mathrm{e}^{\frac{ik_0}{2z}\left[(x-x_0)^2+(y-y_0)^2\right]}dx_0dy_0. \tag{S7}$$

The intensities for 0^{th}, $+1^{\mathrm{st}}$ and -1^{st} orders are

$$I_y=\frac{p'}{2}\cos^2(\frac{\Gamma}{2})\left[a_{\mathrm{L}}^2+a_{\mathrm{R}}^2-2a_{\mathrm{L}}a_{\mathrm{R}}\cos(\Delta\varphi-2\theta)\right] \tag{S8}$$

$$I_y^{+1}=\frac{pa_{\mathrm{L}}^2}{2}\sin^2(\frac{\Gamma}{2}) \tag{S9}$$

$$I_y^{-1}=\frac{pa_{\mathrm{R}}^2}{2}\sin^2(\frac{\Gamma}{2}) \tag{S10}$$

respectively. Here, p and p' are parameters related to propagating distance.[9]

Supplementary Note 2: The proposed polarimetry for polarization detection.

2.1 Photos of the proposed polarimetry.

The size of the glass substrate is 22 mm × 22 mm × 0.17 mm. Figure S1 (a, b) shows the front and side views of the polarimeter, respectively. The thickness of the device was measured as 0.80 mm.

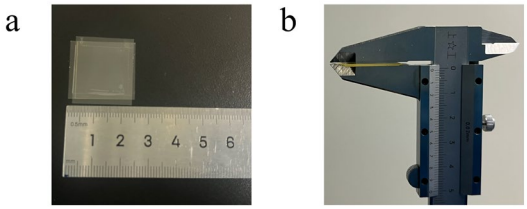

Figure S1. Photos of the proposed polarimeter. The (a) front view and (b) side view of the polarimeter.

2.2 The polarization detection results at different wavelength.

To demonstrate the broadband feasibility of polarization detection, we insert a polarizer before the LC cascaded polarimeter to generate *x* or *y* linear polarization. Corresponding diffraction patterns at different wavelengths from 470 nm to 830 nm are captured, as shown in Figure S2(a-b). The reconstructed polarization states are described by polarization ellipses. The blue and red ellipses represent the L- and R-handed polarizations, respectively. The calculation results are consistent with incident polarization states, proving the effective operation of the LC cascaded polarimeter across the entire visible spectrum.

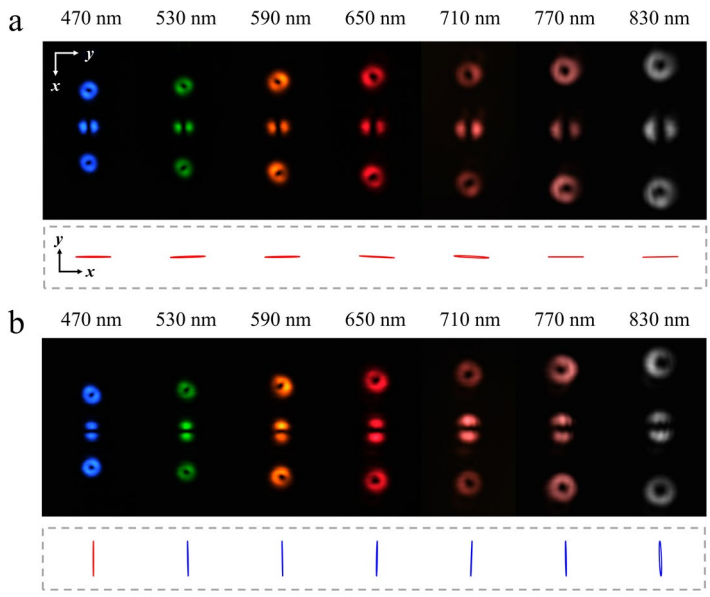

Figure S2. Polychromatic diffraction patterns and corresponding polarization detection results for *x*-polarization (a) and *y*-polarization (b).

2.3 Experimental and simulated results of Stokes parameters of a rotated HWP and a rotated QWP

We initially used a half-wave plate (HWP) to control the polarization of incident light. By varying the orientation angle α_{HWP} of the HWP's fast axis from 0° to 90° in 15° increments, we generated linearly polarized light with an electric field orientation that rotated from the *x*-axis to the *y*-axis and then to the −*x*-axis, in 30° steps. Additionally, we employed a quarter-wave plate (QWP) to further control the incident polarization. The orientation angle α_{QWP} of the QWP's fast axis was varied from −45° to 45° in 15° increments. This adjustment produced a gradual transition in the polarization state, starting from LCP, moving through linear polarization along the *x*-axis, and ending with RCP. Table S1 shows the $\Delta\varphi$ and r we tested, as well as the calculated Stokes parameters S_1 S_2 S_3, and the Stokes parameters S_1 S_2 S_3 measured by a commercial polarimeter. Figures S2 (a-c) present, as the HWP is rotated, the theoretical Stokes parameters (curves), measured Stokes parameters by commercial polarimeter and proposed polarimeter, while Figures S2 (d-f) illustrates the corresponding parameters when the QWP is rotated.

Table S1. Detail test results.

Test results with proposed polarimeter of HWP							
α_{HWP}	0	15	30	45	60	75	90
$\Delta\varphi$	0.070	1.047	2.094	3.037	4.259	5.271	0.000
r	1.067	0.991	0.916	0.907	0.963	1.042	1.078
S_1	0.995	0.500	-0.498	-0.990	-0.438	0.529	0.997
S_2	0.070	0.866	0.863	0.104	-0.898	-0.847	0.000
S_3	-0.064	0.009	0.088	0.098	0.037	-0.042	-0.075
Test results with commercial polarimeter of HWP							
S_1	0.999	0.495	-0.51	-0.999	-0.49	0.489	0.999
S_2	0.021	0.867	0.855	-0.013	-0.879	-0.871	-0.011
S_3	-0.011	0.012	0.041	0.062	0.073	0.051	0.012
Test results with proposed polarimeter of QWP							
α_{QWP}	-45	-30	-15	0	15	30	45
$\Delta\varphi$	5.236	5.201	5.620	0.000	0.524	0.803	4.049
r	17.977	3.683	1.718	0.973	0.550	0.240	0.054
S_1	0.055	0.237	0.685	1.000	0.732	0.315	-0.067
S_2	-0.096	-0.447	-0.535	0.000	0.422	0.326	-0.085
S_3	-0.994	-0.863	-0.494	0.028	0.535	0.891	0.994
Test results with commercial polarimeter of QWP							
S_1	-0.053	0.221	0.754	0.999	0.752	0.253	0.044
S_2	-0.023	-0.467	-0.439	0.022	0.443	0.423	0.001
S_3	-0.998	-0.856	-0.488	-0.012	0.487	0.869	0.999

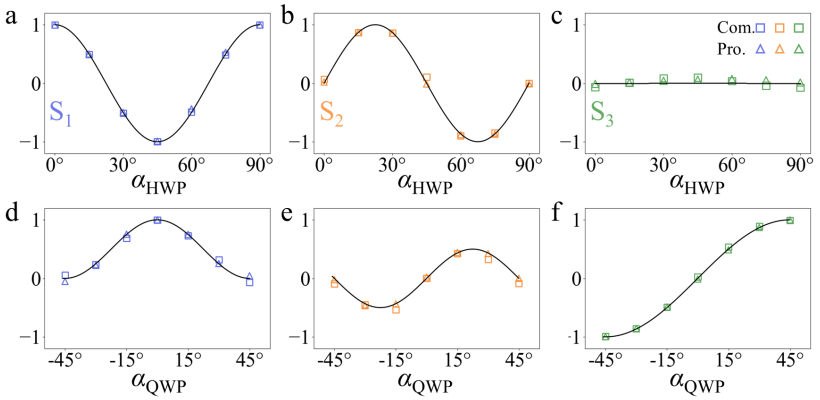

Figure S3. Stokes parameters S_1, S_2, and S_3 when rotating HWP and QWP. The curves represent the theoretical value of Stokes parameters. Measured Stokes parameters by commercial polarimeter and proposed polarimeter is depicted by rectangle and triangle.

Supplementary Note 3: The *q*-plate array for polarization imaging.

3.1 Experimental setup for polarization imaging

To demonstrate the feasibility of polarization imaging, we establish an experimental setup (as shown in Figure S4). The light beam emitted from an LED is expanded and collimated using a beam expander (BE). This expanded beam is then passed through a spectral filter (FBH490-10, Thorlabs, U.S) to narrow the wavelength range of the light. The *q*-plate array is used for acquiring phase information at different positions. For easy demonstration, the LC *q*-plate array which satisfies the 490 nm half-wave condition is made up with LC polymer (OCM-A1, Raito Materials Technology Co., China). The diffraction pattern is collected by a lens (OLD2444-T2M, JCOPTIX, China) and recorded by a CCD (AIC-401GC-USB, JCOPTIX, China).

It is worth noting that a lens inserted between *q*-plate array and LCPG the experimental setup for polarization imaging. Herein, to obtain a clear image for polarization analysis, the *q*-plate array is placed before the lens and imaged onto CCD. And LCPG is used to separate images to the three images. Therefore, the thickness of polarization imaging is no longer as thin as 0.80 mm. The introduction of thickness restrictions mainly depends on the bulky lens, which can be replaced with a polarization independent planar lens.

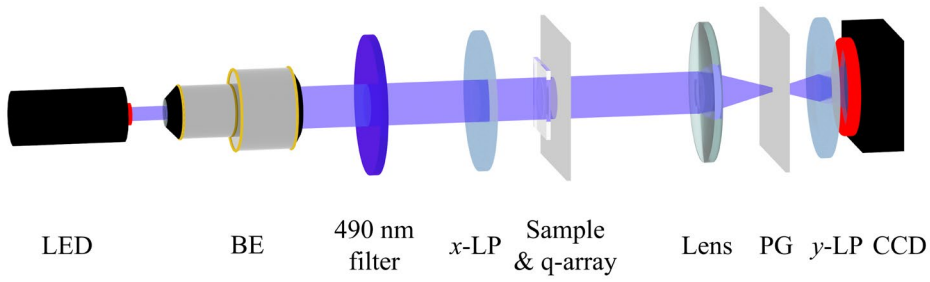

Figure S4. Experimental setup for polarization imaging. BE: beam expander, *x*-LP: linear polarizer with transmission polarization direction along the *x*-axis, *y*-LP: linear polarizer with transmission polarization direction along the *y*-axis.

3.2 Method for data analysis

For data analysis purposes, we wrote a code for reading out the angle between the intensity minima and *x*-axis on OV at 0^{th} order and integrating the intensity inside the entire OV at $\pm 1^{st}$ orders. The captured diffraction patterns are first divided into three parts in Figure S5 (a-c) according to their

spatial positions. As for the 0^{th} order in Figure S5 (b), the original digital image's central point of each *q*-plate is found out firstly. By calculating the intensity minima along each vortex, the angle of each dark branches can be calculated and marked as white lines in Figure S5 (e). [34] The ±1st orders generated by the *q*-plate array (Figure S5 (a, c)) are divided individually and marked with red squares. The whole intensity of each red square region is obtained by summing up the grayscale values correspondingly in Figure S5 (d, f). The chiral amplitude contrast and the chiral phase difference can be calculated out with the patterns.

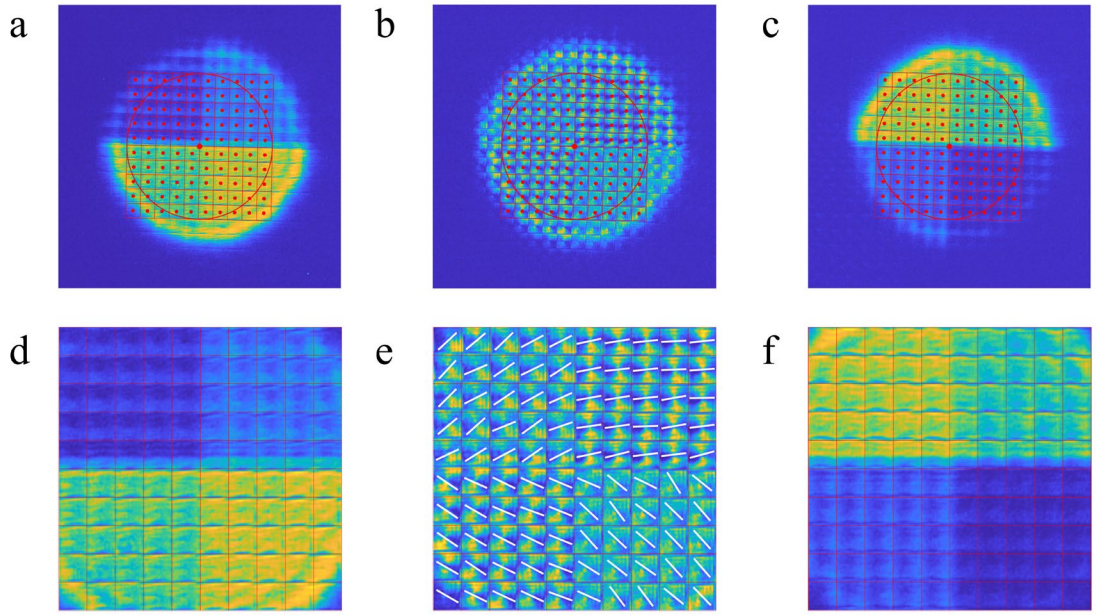

Figure S5. Program for pixel-based image information processing. (a-c) Three parts of the pattern separated from the original picture and the corresponding processed result (d-f).

3.3 Simulation results of patterned phase retarder

To verify the accuracy of our method with *q*-plate array, we simulated the process with the Rayleigh-Sommerfeld vector diffraction theory. By patterning the fast axis orientation of HWP located after *x*-polarization, we can get linear polarized light with different orientations in Figure S6 (a). The Figure S6 (b, c) is the corresponding simulation pattern and their calculation results. By patterning the fast axis orientation of QWP located after *x*-polarization, we can get different chiral polarization states. The Figure S6 (e, f) is the corresponding simulation pattern and their calculation results. We have verified the accuracy of this method by comparing the calculated understanding results with the theoretical incidence results.

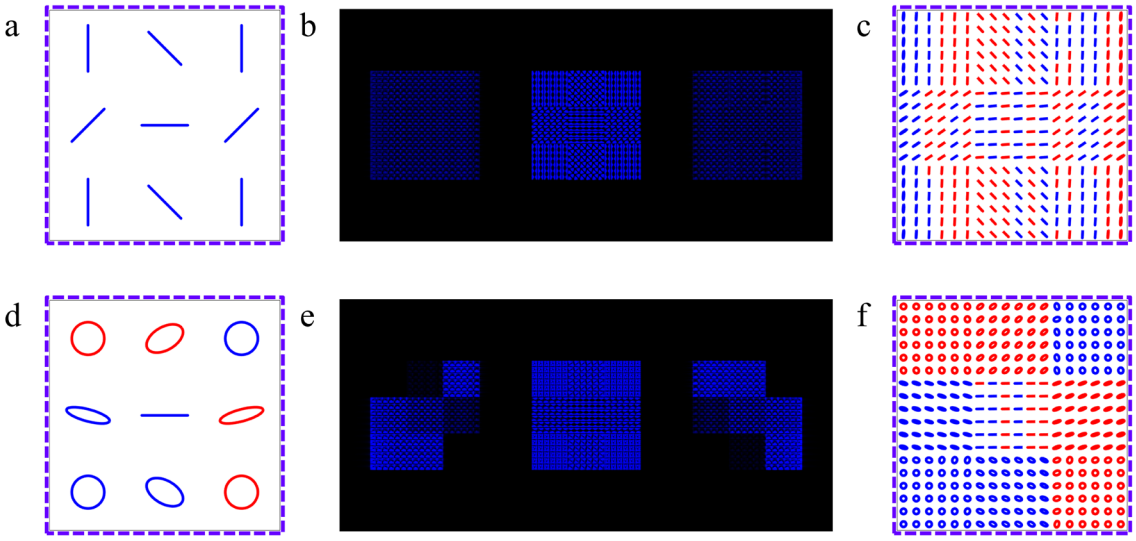

Figure S6. Simulation results of complex polarization patterns, Theoretical polarization distribution (a, d) and their corresponding patterns (b, c) and calculation results (c, f).